# APPLICATIONS OF RAMAN SPECTROSCOPY IN ELECTROCHEMISTRY

R. P. VAN DUYNE

Department of Chemistry, Northwestern University
2145 Sheridan Road, Evanston, Illinois 60201 U. S. A.

**Résumé.** — Dans cet article on résume les caractéristiques de spectroscopie Raman de résonance (SRR) qui permettent le couplage simple d'une méthode de détection spectroscopique vibrationnelle avec une méthode de génération électrochimique. Les applications de cette technique pour observer les ions radicaux régénérés électrolytiquement dans la masse de la solution ainsi que dans la couche de diffusion de l'électrode sont discutées. Enfin un nouveau mécanisme d'exaltation de l'intensité Raman qui permet l'observation des molécules adsorbées sur la surface d'une électrode sera décrite.

**Abstract.** — In this paper we review the characteristics of resonance Raman spectroscopy (RRS) which permit the simple coupling of a vibrational spectroscopic detection method with an electrochemical generation method. The applications of this approach to observing radical ions electrolytically generated in bulk solution as well as in the electrode diffusion layer are discussed. Finally, a new Raman intensity enhancement mechanism which permits one to observe the spectra of molecules adsorbed on an electrode surface will be described.

1. **Introduction.** — Interest in the mechanisms of electrochemical reactions which occur at the interface between an electrically conducting solid and a moderately polar liquid has brought about the development of a number of spectroelectrochemical techniques to probe this interesting and unique chemical environment. The *raison d'etre* of these spectroelectrochemical techniques is to provide superior molecular specificity with respect to the usual electrochemical observables (e. g., current, charge, potential, frequency, time, etc.) for the purposes of : 1) identification and/or detection ; 2) molecular and electronic structure characterization ; and 3) kinetic monitoring of electrogenerated species in any or all of the usual electrochemical environments (viz., bulk solution, electrode diffusion layer, electrode surface and double layer region). For the characterization of electrogenerated species in solution, the spectroscopic techniques which have been employed include electronic absorption spectroscopy in the U. V., vis., and NIR regions [1], infrared (IR) spectroscopy [2], electron spin resonance (ESR) spectroscopy [3], and to a lesser extent nuclear magnetic resonance (NMR) spectroscopy [4], and mass spectrometry (MS) [5]. Of these techniques electronic absorption spectroelectrochemistry and ESR spectroelectrochemistry have made the greatest impacts on electrochemical mechanism studies thus far. Although both of these approaches have significant virtues, they also suffer from certain defects ; in many situations the molecular specificity of electronic absorption spectroscopy is insufficient to make a positive identification of an electrogenerated species. In the case of ESR spectroscopy, the molecular specificity is very high but it is only applicable to odd electron species and its ability to easily monitor time dependent electrochemical changes is limited to the time scale of seconds. For the characterization of electrode surfaces and/or the adjacent solution layer, the techniques employed most frequently to date include the *in situ* methods of specular (or internal) reflection spectroscopy [6, 7] and ellipsometry [8] as well as the high vacuum surface techniques of ESCA [9], Auger electron spectroscopy [10], low energy electron diffraction [11], etc. which, of course, are not applicable to the direct study of electrodes immersed in solutions. Although many useful applications of these techniques have been made, they do suffer from either or both lack of molecular specificity or restricted applicability. Consequently there is a motivation for the development of new spectroscopic methods for electrochemical studies which can overcome some of the current limitations of the existing methodology.

For the past few years our research group at Northwestern University [12] as well as a few other groups, primarily in England [13-16], have embarked on a program to evaluate the potential of Raman spectroscopy as a molecularly specific probe of the electrochemical environment. The fundamental problem with normal Raman spectroelectrochemistry is that it must be capable of sufficient sensitivity to observe high S/N spectra for $10^{-3}$ M to $10^{-5}$ M electrogenerated species in bulk solution ; $10^{13}$ to $10^{14}$ molecules, ions, etc., generated in the few micron thick diffusion layer of an electrode ; and ca. $10^{12}$ to $10^{13}$ adsorbed molecules in a monolayer on an electrode surface. Typically the sensitivity of the normal spontaneous Raman process is not sufficient to meet this requirement. To overcome this lack of sensitivity inherent in normal Raman spectroscopy (NRS) we have concentrated our attention on the electrochemical application of reso-

nance Raman spectroscopy (RRS) [12] which is $10^4$ to $10^6$ times more sensitive than NRS. The experiments which have been carried out in our laboratory to date unambiguously show that resonance Raman spectroelectrochemistry (RRSE) has the requisite sensitivity to obtain high quality vibrational spectra for species in all three of the normal electrochemical environments. Following a brief discussion of the characteristics of RRS versus NRS and the apparatus for carrying out RRSE experiments, I will illustrate the applicability of resonance Raman spectroscopy to each of the electrochemical environments with specific examples from our research program.

2. **Characteristics of resonance Raman scattering.** — Both NR and RR spectroscopy involve a light scattering experiment in which a highly monochromatic (monoenergetic) photon beam from a laser is directed at a target species, the inelastically scattered light from the target is collected, and it is wavelength analyzed with a scanning double monochromator. In the NR case only ca. 1 in $10^{10}$ input photons emerges as a Raman shifted output photon. This inefficiency of NR scattering arises fundamentally from the fact that the laser irradiates the target in a transparent region of its electromagnetic spectrum. Thus the laser is only weakly interacting with the target. In Raman spectroscopy the quantum of energy corresponding to the wavelength difference between the incident and scattered radiation also corresponds to a molecular transition of the sample. This transition can be translational (e. g., lattice modes of a crystal), rotational, vibrational, or electronic in nature. In this paper we will be concerned only with vibrational transitions. A schematic representation of a NR vibrational transition and the relationship of the incident laser wavelength to the target molecule's electronic absorption spectrum is shown on the right hand side of figure 1.

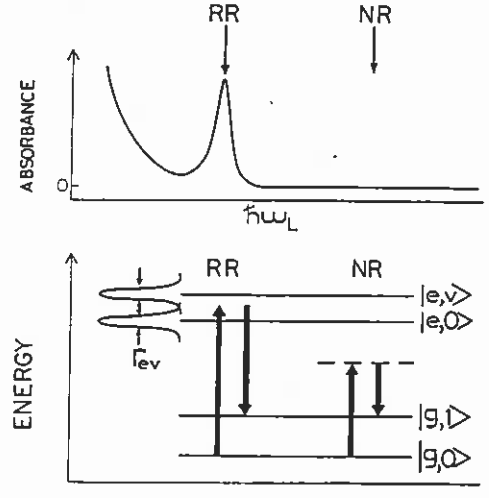


FIG. 1. — Schematic representation of the normal Raman (NR and resonance Raman (RR) scattering processes. Top : electronic absorption spectrum of target species showing position of laser excitation for NRS and RRS. Bottom : Net energy level transitions for a Raman fundamental in NRS and RRS.

Photons are said to be resonantly scattered from the target species when the energy of an incident photon approaches that corresponding to the electronic absorption band of the target. As shown on the left side of figure 1, the net energy level transition of an RR process is the same as that for the NR process. The main difference is that in the RR process the intermediate states are real vibronically excited states of the target rather than virtual states as in the NR case. As a result of the strong interaction between the laser light and the target molecule, the efficiency (i. e., quantum yield) of RR scattering is of the order of $10^4$ to $10^6$ times that of NR scattering. The origin of this increase in scattering efficiency and hence the sensitivity of RR scattering can be more clearly seen by examining the relevant equations which describe the intensity of Raman scattering from an ensemble of randomly oriented target molecules. The total intensity of a Raman line is given by [17]

$$I = KI_L C_i \hbar\omega_s^4 \Phi_s \qquad (1)$$

where the constant $K$ is $8\pi/27\,c^4$, $I_L$ is the intensity of the incident laser light, $C_i$ is the concentration of the target species, $\hbar\omega_s$ is the energy of the Raman scattered photon, and $\Phi_s$ is the Raman scattering efficiency which is in turn given by

$$\Phi_s = \left| \sum_{\rho\sigma} \alpha_{\rho\sigma} \right|^2 \qquad (2)$$

$\alpha_{\rho\sigma}$ is an element of the scattering tensor and $\rho$ and $\sigma$ are the polarizations of the Raman and incident light respectively. In terms of second order, time-dependent perturbation theory, $\alpha_{\rho\sigma}$ for a net transition from the 0th vibrational level of the ground electronic state, $g$, to the 1st vibrationally excited level of g is given by [17, 18]

$$\alpha_{\rho\sigma} = \sum_{e,v} \frac{\langle 0, g \mid \rho \mid e, v \rangle \langle v, e \mid \sigma \mid g, 1 \rangle}{(E_{ev} - E_{g0}) - \hbar\omega_L - i\Gamma_{ev}} + \frac{(\rho \leftrightharpoons \sigma)}{(E_{ev} - E_{g1}) + \hbar\omega_L - i\Gamma_{ev}}. \qquad (3)$$

When $\hbar\omega_L \ll (E_{ev} - E_{g0})$ we are in the NR regime, $\alpha_{\rho\sigma}$ is small, and consequently $\Phi_s$ takes on a value of ca. $10^{-10}$. When $\hbar\omega_L$ approaches the value of a molecular resonance $(E_{ev} - E_{g0})$, the denominator of the first term in equation (3) becomes small (i. e., limited only by the homogeneous line width of the resonant level $\Gamma_{ev}$) and consequently the first term dominates the scattering tensor expression. In resonance scattering the corresponding value of $\Phi_s$ can be as high as $10^4$ to $10^6$ times that in the NR case. The magnitude of the enhancement is thus seen to depend on the *degree of resonance* between the laser light and the real vibronic levels of the target ; but, in addition it should be noted that the magnitude of the numerator of equation (3), which is effectively the extinction coefficient of the target at the laser excitation wavelength, also determines the size of the enhancement. In general one

notes that the stronger the extinction coefficient of the target species the greater will be the resonance enhancement factor.

From the foregoing discussion it can clearly be seen that the laser excitation wavelength plays a much more significant role in determining the nature of RRS than of NRS. Consequently the ability to tune the excitation laser to a particular part of a molecule's electronic absorption spectrum rather than to rely on the chance coincidences that occur when fixed frequency lasers are employed will be of particular benefit to the experimentalist. Furthermore in order to make as many molecules as possible accessible to examination by RRS, it will be necessary to use uv and near I. R. lasers as well as visible lasers. With such broad frequency coverage of laser excitation wavelengths, it will also be possible to study the R R spectrum of the same molecule exciting into different electronically excited states. As we will see later in this paper, vastly different R. R. spectra can result by exciting into different excited electronic states of the same target species. In addition it should be pointed out that in cases where $\Gamma_{ev}$ is narrow relative to the energy difference between $(E_{ev}\text{-}E_{g0})$ and $\hbar\omega_L$, it will be of advantage to tune the laser within an electronic absorption band to map out the resonance Raman excitation spectrum (profile) of a particular normal mode [19] as well as to seek excitation wavelengths which maximize the sensitivity of the R R technique for detection purposes such as in electrochemical applications.

Resonance Raman spectra differ from normal Raman spectra in ways other than in intensity. The most striking difference is that not all of the N R active vibrational modes undergo the large resonance enhancement effect. In the simplest case of small molecules where only one electronically excited state of the target is coupled in to the excitation laser and that state is not vibronically coupled to another of different symmetry, only the totally symmetric vibrational modes are resonance enhanced. This situation is easily detected since the depolarization ratio for a resonance enhanced totally symmetric mode is usually 1/3 [20]. Nontotally symmetric normal modes can be resonance enhanced if, for example, they are involved in vibronic coupling of two electronic states of different symmetry and in which one of the states is pumped by the excitation laser. In this circumstance any vibrational symmetry contained in the direct product of the electronic state symmetries can undergo resonance enhancement [21]. Nontotally symmetric modes usually have depolarization ratios $\leqslant 3/4$ and this serves as a means for their distinction from totally symmetric modes and as a means for detecting vibronic coupling. In the special case of a large macromolecule containing a chromophore which can be RR excited, another reason exists for the observation of only a subset of the Raman active modes. Only those vibrations associated with the chromophore of a macromolecule will exhibit R R enhancement. This feature of RRS has been exploited with great success to simplify the otherwise hopelessly complex Raman spectra of biologically significant molecules (e. g., enzymes, heme proteins, etc.) [22]. Another major difference between RR spectra and NR spectra is that the observation of high intensity overtone progressions and combination bands is a frequent occurence in RRS whereas it is comparatively rare in NRS. Careful analysis of the intensity pattern contained in an overtone progression can lead to information about the extent of distortion in the observed normal coordinate in the resonantly excited state as compared to the ground electronic state [23, 24].

3. **Experimental apparatus.** — The electrochemical cell and general optical configuration for carrying out RRSE experiments in bulk solution using controlled potential bulk coulometry as the electrogeneration mode is shown in figure 2 A. There are no special

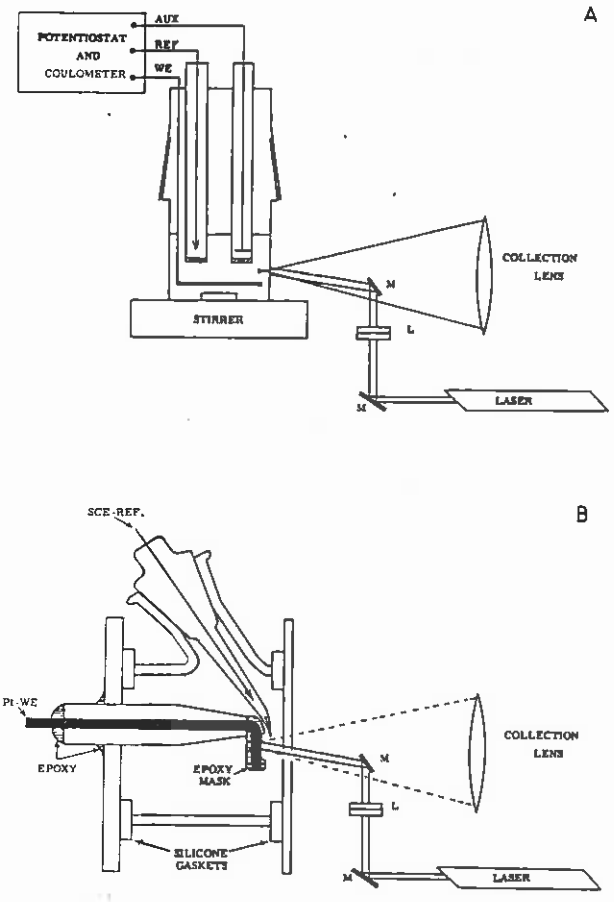


FIG. 2. — Resonance Raman spectroelectrochemistry cells and backscattering optical geometry : A) controlled potential electrolysis cell for bulk solution experiments ; B) cell for diffusion layer and electrode surface experiments.

design requirements for the cell except that one of its walls be transparent to both the laser excitation and Raman scattered wavelengths. In a bulk electrolysis experiment, a solution originally $10^{-5}$ to $10^{-3}$ M in electroactive species is converted quantitatively by an

oxidation or reduction reaction of $10^{-5}$ to $10^{-3}$ M RR active product. In this approach the electrogenerated product must be stable for the duration of the monochromator scan (ca. 1 hour for a full 100 $cm^{-1}$ to 3 000 $cm^{-1}$ scan) if one is not to observe spurious bands in the resulting spectrum. Consequently reversal coulometry is used to demonstrate the requisite stability for the test substance. A back scattering optical geometry has been found to be most convenient for this experiment. The collection lens focuses the Raman scattered light back on to the entrance slit of a double monochromator used to wavelength analyze the inelastically scattered light. Figure 2 B shows the electrochemical cell used for RRSE experiments in which the target species is confined either to the electrode diffusion layer or is adsorbed on the electrode surface. A similar backscattering optical geometry is employed for this cell.

A block diagram of the overall computer controlled RRSE instrumentation system is shown in figure 3.

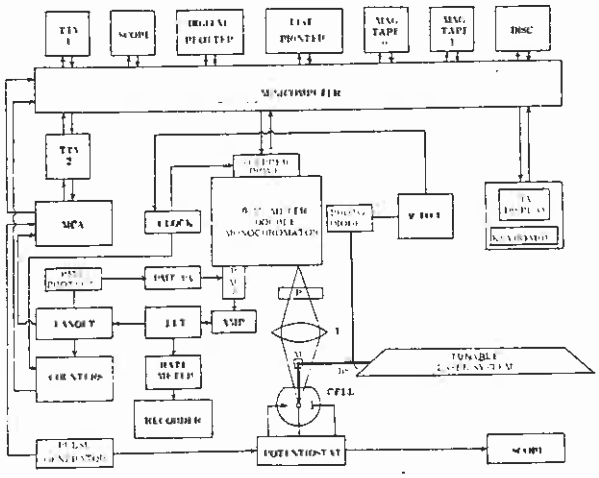

FIG. 3. — Schematic diagram of the resonance Raman spectro-electrochemistry system.

The computer is a 32 K Raytheon 500 system outfitted with the peripherals shown. The Raman spectrometer system is of conventional design except that it is fitted with widely tunable laser sources and is connected to a multichannel analyzer (MCA) used to collect electrochemically initiated Raman transients. The laser system consists of CW argon ion and dye lasers, a flashlamp pumped pulsed dye laser, and nonlinear frequency doubling crystals for generating ultraviolet laser excitation wavelengths. With this system, laser excitation can be accomplished at the following frequencies : 2 572 Å, 2 600-3 500 Å, 3 511 Å, 3 638 Å, and 4 350-7 500 Å. It should be pointed out that with the addition of either a frequency tripled Nd : YAG laser pumped dye laser or a nitrogen laser pumped dye laser that the gap between 3 500 and 4 350 Å could be closed with a tunable source. Also it is now possible to generate tunable near ir wavelengths using either a 4 W CW $Kr^+$ laser pumped dye laser [25] or a Nd : YAG pumped optical parametric oscillator [26]. With such additions we would have complete RR excitation of most of the uv, all of the visible, and some of the near ir spectrum.

**4. Resonance Raman spectroscopy of radical ions in bulk solution and in the electrode diffusion layer.** — The objectives in RRSE studies of radical ions are : 1) to identify the RR active vibrational modes of the electronic ground state of an electroactive molecule, R, that are most sensitive to the electronic structure changes that occur during electron transfer reactions such as :

$$^1R + e^- \rightleftharpoons {}^2R^- \quad \text{and} \quad {}^1R \rightleftharpoons {}^2R^+ + e^- \qquad (4)$$

and 2) to use the RR effect to reveal some of the excited state properties of radical ions which have, heretofore, been hidden by virtue of the fact that radical ions are nonluminescent entities. Achieving the first of these objectives will provide some of the fundamental information necessary for the theoretical and experimental evaluation of the role of intramolecular vibrational energy dissipation pathways in exothermic electron transfer processes [27-31]. Achieving the second objective will provide excited state electronic structure information which should be useful in evaluating the chemical accuracy of molecular orbital calculations on open shell species. In the first part of this section, I will describe RRSE experiments for stable radical ions in bulk solution using the controlled potential coulometry electrogeneration mode and in the second part I will describe an alternative method for making time resolved RRSE measurements on species which are stable on the tens of millisecond to seconds time scale but would not be sufficiently stable to enable RR to be observed by the bulk solution technique without the risk that some of the observed lines might be due to decay products.

4.1 BULK SOLUTION RRSE STUDIES. — To illustrate the use of bulk solution RRSE measurements made with the cell and apparatus pictured in figure 2 A, I will take as an example our studies on tetracyanoquinodimethane$^-$ ($TCNQ^{\cdot-}$) and on the radical cation of tetrathiafulvalene ($TTF^{\cdot+}$). The structures of these two species are pictured below. These particular dou-

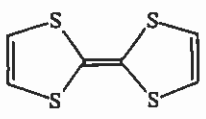

TTF

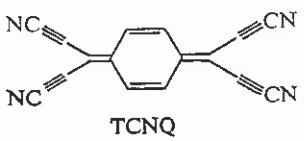

TCNQ

blet ground state ions were chosen for study because : 1) their lifetimes are in excess of several hours when electrogenerated in acetonitrile containing 0.1 M tetrabutylammonium perchlorate (TBAP) as supporting electrolyte, 2) they have intense visible and near uv absorption spectra that are overlapped by our

$Ar^+$ and dye lasers as shown in figure 4, and 3) they are intermediately sized species between the diatomics such as $I_2$ [32], small inorganic anions such as $MnO_4^-$ [23] and the large biomolecules such as heme proteins

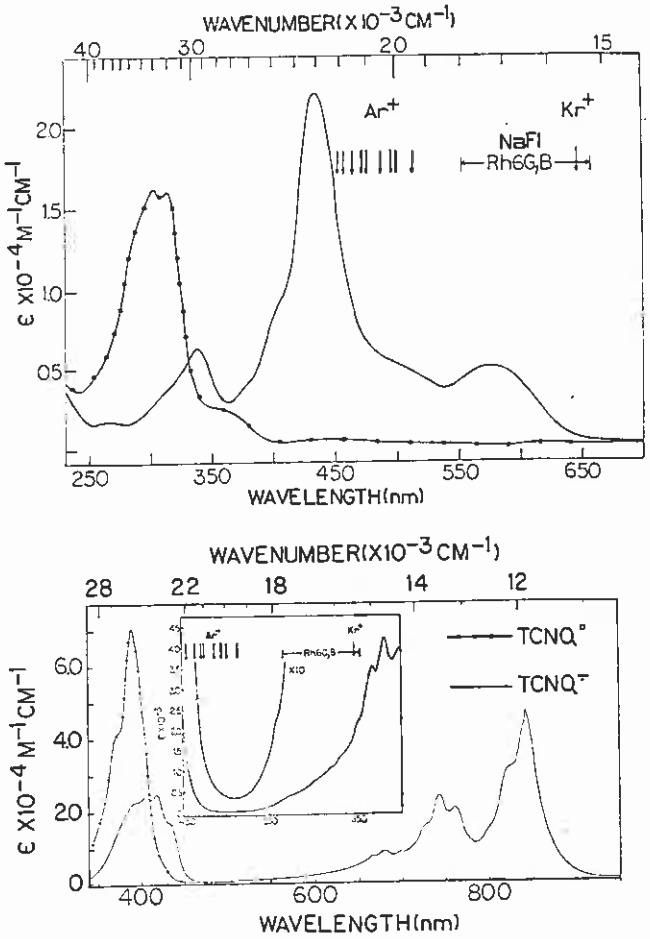


FIG. 4. — Electronic absorption spectra. Top : TTF-$h_4$ and TTF-$h_4^+$ from 250-650 nm. (●—●—●) TTF-$h_4$ in acetonitrile. (————) TTF-$h_4^+$ electrogenerated at +0.50 V *vs.* SCE in acetonitrile containing 0.10 M TBAP [TTF-$h_4^+$] = 4.38 × $10^{-4}$ M; cell pathlength = 0.10 cm. Bottom : TCNQ and $TCNQ^-$ from 350-950 nm. (●—●—●—●) TCNQ in acetonitrile. (————) $TCNQ^-$ electrogenerated at +0.00 V *vs.* SCE in acetonitrile containing 0.10 M TBAP. [$TCNQ^-$] = 1.40 × $10^{-4}$ M ; cell pathlength = 0.10 cm. The inset figures show the $TCNQ^-$ absorption spectrum from 450 to 700 nm. with two different expanded extinction coefficient scales in the region of spectral overlap with the fixed frequency ion laser lines ($Ar^+$ and $Kr^+$) and the CW dye laser tuning range for sodium fluorescein (NaFl), rhodamine 6G (R6G), and rhodamine B (RB) dye solutions.

[22] which have been studied by RRS previously. It should be noted that the $Ar^+$ laser and CW dye lasers overlap the electronic absorption spectra of these ions in different electronic states of the same radical ion. Furthermore it should be noted that these ions are effectively ideal target species for RR examination since there is virtually no possibility of concomitantly exciting broad band molecular fluorescence. The unpaired electron in a radical ion creates a large spin-orbit coupling interaction which in turn gives rise to either fast doublet-quartet intersystems crossing or doublet-doublet internal conversion rather than doublet-doublet fluorescence.

Let us first consider the RRS of the

$$TCNQ + e^- \rightleftharpoons TCNQ^-$$

system ($E^0$ = + 0.20 V *vs.* SCE). Figure 5 shows a preresonance Raman spectrum of 10.9 mM neutral

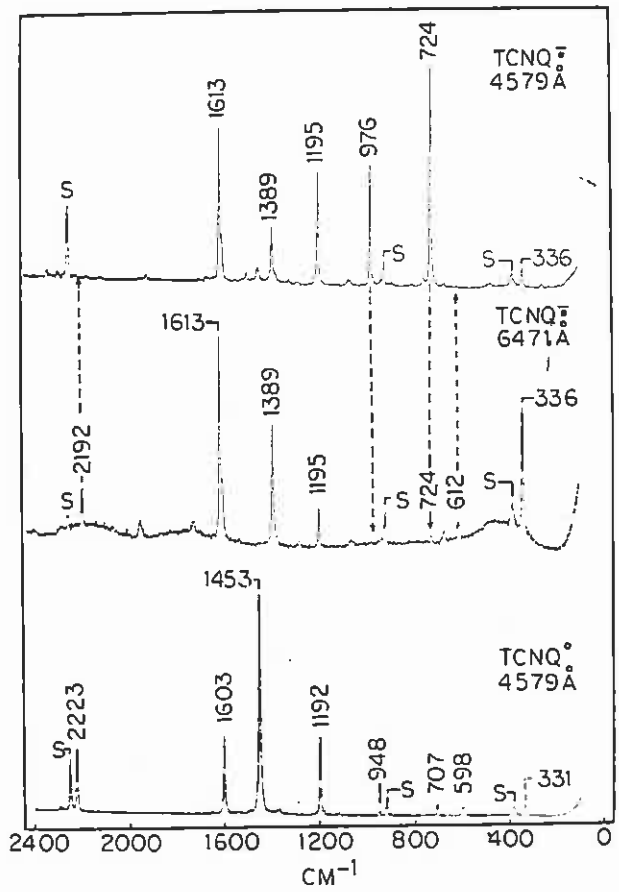


FIG. 5. — Resonance Raman spectra of electrogenerated $TCNQ^-$ and preresonance Raman spectrum of $TCNQ^0$. The $TCNQ^-$ was electrogenerated by controlled potential coulometry at — 0.10 volt *vs.* SCE in 0.1 M TBAP/$CH_3$ CN. Top : $TCNQ^-$ (3.00 mM) excited at 4 579 Å, scanned at 0.333 Å $s^{-1}$ in second order, 1.00 s. counting interval, laser power 10 mW, bandpass = 2.0 $cm^{-1}$ in second order. Plasma lines were removed with an interference filter. Center : $TCNQ^-$ (2.24 mM) excited at 6 471 Å, scan rate 0.333 Å $s^{-1}$ in first order, 1.00 s. counting interval, laser power = 74 mW, bandpass = 2.2 $cm^{-1}$. $Kr^+$ plasma lines were removed with a Claasen filter. Bottom : $TCNQ^0$ (10.9 mM) excited at 4 579 Å, scan rate 0.333 Å $s^{-1}$ in second order, 1.00 s. counting interval, laser power = 20 mW, bandpass = 1.2 $cm^{-1}$ in second order. S denotes a NR solvent band. No NR bands due to supporting electrolyte were observed.

TCNQ in $CH_3CN$ solution excited with the 4 579 Å $Ar^+$ laser line, a resonance Raman spectrum of 2.24 mM $TCNQ^-$ electrogenerated in $CH_3CN$ containing 0.2 M TBAP and excited with the 6 471 Å $Kr^+$ laser line [33], and a resonance Raman spectrum

of 3.00 mM $TCNQ^{\cdot-}$ electrogenerated in $CH_3CN$/0.1 M TBAP and excited with the 4 579 Å $Ar^+$ laser line [34]. It should be noted that the 6 471 Å line excites $TCNQ^{\cdot-}$ in the region of a transition to an upper vibronic level of its lowest excited state and that the 4 579 Å line excites it in the region of the 0-0 transition of its next highest excited state. The assignments of the observed lines in these spectra has been given in detail elsewhere [24, 33]. However certain important vibrational bands will be identified here. In the TCNQ neutral spectrum the 2 223 $cm^{-1}$ band is the $\nu_2 C = N$ totally symmetric stretch and the 1 453 $cm^{-1}$ band is the $\nu_4$ exocyclic C = C totally symmetric stretch. These bands are identified because they undergo the largest frequency shift upon conversion to $TCNQ^{\cdot-}$ (viz., $\nu_2 = 2\,192$ $cm^{-1}$ and $\nu_4 = 1\,389$ $cm^{-1}$). Thus one of the most important pieces of chemical information which the RRSE technique provides directly is the identification of the vibrational modes most sensitive to the changes in electronic structure caused by a one-electron transfer reaction. Another important feature to observe about these spectra is that the C ≡ N of the dilute solute molecule is clearly resolved from the C ≡ N in the 19 M $CH_3CN$ solvent. Comparison of the intensity of the solvent C ≡ N band with that of the solute gives a rough indication of the magnitude of the resonance enhancement effect. Perhaps the most striking feature of these spectra is the comparison between the $TCNQ^{\cdot-}$ RR spectra obtained by excitation with the 4 579 Å and the 6 471 Å lines. These spectra are vastly different. The C ≡ N band is totally absent in the *blue* spectrum and the weak lines at 976 $cm^{-1}$ and 724 $cm^{-1}$ in the *red* excited spectrum are some of the strongest lines in the *blue* spectrum. The qualitative conclusion that can be drawn for this comparison is that in order to derive the full complement of vibrational information from the RR technique, in particular applied to the study of relatively small ions and molecules, the target species must be excited in as many of its excited states as possible. This implies that widely tunable laser sources must be used for this type of work. Imagine the chagrin of an analytical chemist asked to determine whether an unknown radical ion ($TCNQ^{\cdot-}$) contained a C ≡ N functional group if he only had an $Ar^+$ laser (none of the other $Ar^+$ laser lines resonantly enhance the $TCNQ^{\cdot-}$ C ≡ N mode either). In addition a more quantitative statement can be made particularly about the C ≡ N vibration in comparing the *red* and *blue* excited $TCNQ^{\cdot-}$ spectra. As indicated in section II the amount of resonance enhancement of a particular vibration depends on two factors : 1) the smallness of the denominator and 2) the largeness of the numerator in equation (3). A more detailed analysis of the numerator reveals that it contains a Franck-Condon factor [18]. It is well known that the Franck-Condon factor associated with a vibronic transition is zero unless there is a difference between the value of the equilibrium nuclear position of the observed normal mode in the excited state and the ground state. We interpret the fact that one dœs not see resonance enhancement of the C ≡ N vibration in $TCNQ^{\cdot-}$ with *blue* excitation as a manifestation of the fact that the value of the equilibrium nuclear position of the C ≡ N mode (i. e., approximately the C ≡ N bond length since $\nu_2$ is essentially a pure normal mode consisting of only one internal coordinate) in the second excited state is virtually identical to that in the ground electronic state. This in turn makes the Franck-Condon factor for this mode approximately equal to zero and therefore the numerator of equation (3) is very small. Similarly this interpretation suggests that the distorsion of the equilibrium nuclear positions in the 976 $cm^{-1}$ and 724 $cm^{-1}$ normal modes is greater in the second excited state relative to the ground state than in the first excited state. A more quantitative analysis of this interpretation will be presented elsewhere. Before going on to consider the RRS of a cation radical, I would like to emphasize that in RRS it is not necessary to achieve an exact coincidence between the exciting laser line and the wavelength corresponding to the maximum of an electronic absorption band. These high S/N ratio RR spectra for $TCNQ^{\cdot-}$ were obtained at excitation wavelengths where the extinction coefficient of the resonant scatterer was only 700-2 000 $M^{-1}$ $cm^{-1}$. In general the *rule of thumb* is that a reasonable quality spectrum can be obtained in an RRS experiment if the extinction coefficient at the laser exciting frequency is at least 500 $M^{-1}$ $cm^{-1}$ for a bulk concentration of the RR scatterer of ca. 2 mM.

As an example of an RRSE study on a cation radical, let us discuss the $TTF \rightleftharpoons TTF^{\cdot+} + e^-$ system ($E^0 = +0.31$ V *vs.* SCE). Figure 6 shows the NR spectrum of solid TTF neutral excited with a 6 000 Å rhodamine 6 G (R6G) CW dye laser, a RR spectrum of 1.0 mM $TTF^{\cdot+}$ electrogenerated in $CH_3CN$/0.1 M TBAP and excited with the R6G dye laser tuned to 5 800 Å, and a RR spectrum of 1.00 mM electrogenerated $TTF^{\cdot+}$ excited with the 4 579 Å Ar + laser line. The 6 000 Å excitation wavelength for the NR spectrum of $TTF^0$ was chosen to avoid exciting the broad band fluorescence of some minor impurity in the solid. The 5 800 Å dye laser excitation wavelength was chosen to coincide with the absorption maximum of the lowest energy absorption band of $TTF^{\cdot+}$ (see figure 4) while 4 579 Å excites $TTF^{\cdot+}$ on the low energy side of the intense central absorption band peaked at 435 nm. Detailed assignments of the Raman lines in $TTF^0$ [24, 35] and in $TTF^{\cdot+}$ [24] have been given elsewhere. For the purposes of this paper, we will comment on the electronic structure sensitive modes of TTF. It will be observed that the 1 513 $cm^{-1}$ band of $TTF^0$ shifts by 86 $cm^{-1}$ to 1 427 $cm^{-1}$ in the radical cation. This mode is the central C = C totally symmetric stretch (actually it is a linear combination of the central C = C double bond and the ring C = C double bond with the

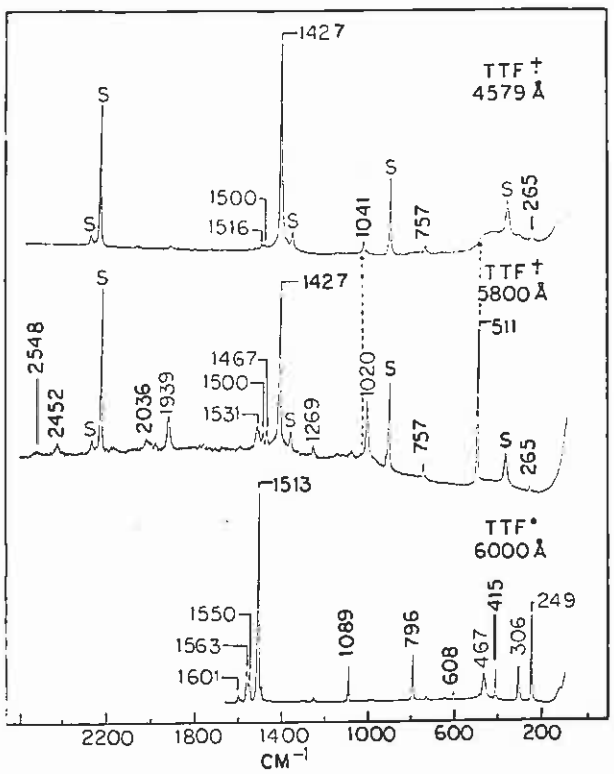


FIG. 6. — Resonance Raman spectra of electrogenerated TTF-$h_4^{+\cdot}$ and normal Raman spectrum of TTF-$h_4$ solid. The TTF-$h_4^{+\cdot}$ (1.0 mM) was electrogenerated by controlled potential coulometry at + 0.50 V *vs.* SCE in 0.1 M TBAP/$CH_3CN$. Top: TTF-$h_4^{+\cdot}$ excited at 4 579 Å, scanned at 0.333 Å/s. in second order, 1.00 s. counting interval, laser power = 70 mW, bandpass = 2.0 $cm^{-1}$ in second order. Plasma lines were removed with an interference filter. Center: TTF-$h_4^{+\cdot}$ excited at 5 800 Å, Rh 6G, scan rate = 0.333 Å/s., 1.00 s. counting interval, laser power = 90 mW, bandpass = 3.0 $cm^{-1}$. Bottom; TTF-$h_4$ powder excited at 6 000 Å, scan rate = 0.333 Å/s., 1.00 s. counting interval, laser power = 30 mW, bandpass = 1.2 $cm^{-1}$.

central C = C predominating). The other strongly electronic structure sensitive mode is the 467 $cm^{-1}$ C-S stretch in the neutral which shifts to 511 $cm^{-1}$ in the cation radical. Both of these shifts are in accord, in magnitude as well as direction, with the corresponding bond order changes calculated within the framework of the PPP-MO scheme [36]. The most striking features of the TTF$^{+\cdot}$ RR spectra are: 1) in the spectrum excited at 5 800 Å a high intensity overtone progression is observed for the 511 $cm^{-1}$ C-S totally symmetric stretch fundamental (viz. $\nu_{C-S}$ = 511 $cm^{-1}$, 2 $\nu_{C-S}$ = 1 020 $cm^{-1}$, 3 $\nu_{C-S}$ = 1 531 $cm^{-1}$, 4 $\nu_{C-S}$ = 2 036 $cm^{-1}$, and 5 $\nu_{C-S}$ = 2 548 $cm^{-1}$) and 2) comparison of the 5 800 Å excited spectrum with the 4 579 Å excited spectrum shows that the distorsion in the C-S bond length of TTF$^{+\cdot}$ in the higher excited state is so much less than in the lowest excited state that not only is the C-S overtone progression absent but the 511 $cm^{-1}$ fundamental itself is absent. A detailed analysis of the Franck-Condon factors associated with the C-S stretch in several TTF-$X_4^{+\cdot}$ (X = H, D, and $CH_3$) derivatives and their structural implications as a function of excitation wavelength has been presented elsewhere [24]. Again the most important qualitative features of these spectra are that the electronic structure sensitive modes of a molecule undergoing a one-electron transfer reaction are directly identified by the RRSE technique and that to obtain all the vibrational information contained in the RR technique one must excite as many electronic states as possible. One final comment is in order concerning the TCNQ$^{-\cdot}$ and TTF$^{+\cdot}$ RRSE experiments. Recently we have been successful in obtaining well resolved RR spectra for the one-dimensional organic electrical conductor TTF-TCNQ in the solid state [24]. Knowledge of the RR spectra of the isolated TCNQ$^{-\cdot}$ and TTF$^{+\cdot}$ radical ions has proved invaluable in the interpretation of such solid state spectra. We expect that RRSE studies coupled with RR spectral studies of charge transfer solids will be a very fruitful area for future investigation.

4.2 DIFFUSION LAYER RRSE STUDIES. — This section describes a time resolved RRSE experiment which employs either of the cyclic potential step electrogeneration waveforms shown in figure 7 and the cell and laser

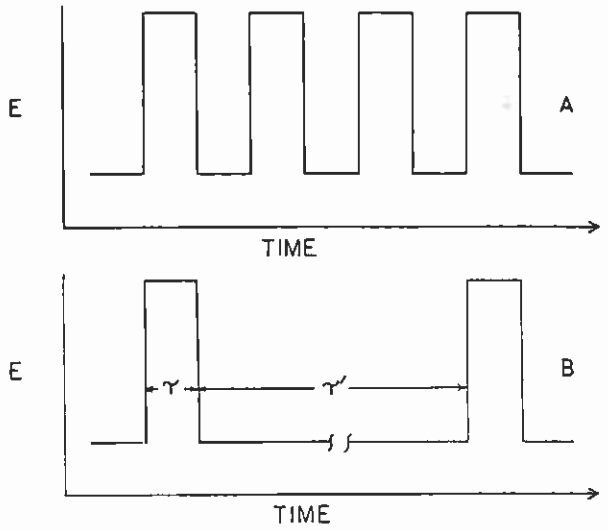


FIG. 7. — Applied potential waveforms used for obtaining: (A) RR scattering spectra of electrogenerated species in the diffusion layer and (B) Signal averaged, double potential step RRI *vs.* time transients of the individual vibrational features in a RR scattering spectrum. Waveform frequencies, pulse switching times, $\tau$, and duty cycles, $\tau'/\tau$, are given in the text.

back-scattering arrangement pictured in figure 2 B [37]. When waveforms of this type are applied through an appropriate potentiostat to a platinum working electrode immersed in an unstirred solution containing electroactive species, solvent, and supporting electrolyte, a steady state concentration profile of a RR active species such as a radical ion can be set up in the electrode's diffusion layer. As an example of such a situation let us consider the one-electron oxidation under cyclic potential step conditions of N, N, N′, N′-

tetramethyl-p-phenylenediamine (TMPD) to form its radical cation (Würster's Blue, $TMPD^{+\cdot}$) :

$$TMPD \rightleftharpoons TMPD^{+} + e^{-} \qquad (5)$$

$$E^{0} = +0.11 \text{ V } vs. \text{ SCE}$$

A schematic representation (actually a concentration profile calculated by finite difference digital simulation for a single cycle of the waveform in figure 7 B) of the steady state concentration profiles of $TMPD^{0}$ and $TMPD^{+\cdot}$ are shown in figure 8. A R6G CW dye laser

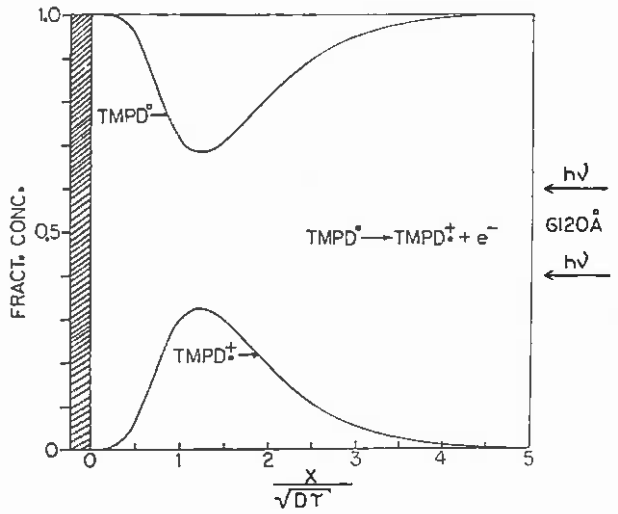


FIG. 8. — Concentration profiles for $TMPD^{0}$ and $TMPD^{+\cdot}$ under cyclic potential step electrogeneration conditions. Distance scale is in dimensionless units of $X/\sqrt{D\tau}$ where $X$ is distance in cm, $D$ is the diffusion coefficient in $cm^{2}$ $s.^{-1}$, and $\tau$ is the applied pulse width in s.

tuned to 6 120 Å which is the absorption maximum of the 0-0 vibronic component of the lowest energy $TMPD^{+\cdot}$ absorption band ($\varepsilon_{6120} = 1.25 \times 10^{4}$ $M^{-1}$ $cm^{-1}$) is used as the excitation source. Since $TMPD^{0}$ absorbs in the uv for $\lambda \leqslant 360$ nm [38], the 6 120 Å R6G laser only excites the electrode reaction product ($TMPD^{+\cdot}$) produced in response to the cyclic potential step waveform. The RR spectrum of $TMPD^{+\cdot}$ confined to the electrode diffusion layer by the waveform of figure 7 A applied at a repetition rate of 10 Hz is shown in figure 9. This spectrum was obtained by scanning the double monochromator for a period of ca. 30 min (50 $cm^{-1}$ $min^{-1}$) while the cyclic potential step waveform was applied to the cell. The normal Raman bands at 379 $cm^{-1}$ and 918 $cm^{-1}$ are from the $CH_3CN$ solvent and the shoulder at 931 $cm^{-1}$ is the NR Cl-O stretch of the TBAP supporting electrolyte. All other bands are the RR features of $TMPD^{+\cdot}$. These lines are all totally symmetric modes since the depolarization ratios were found to be 1/3. A detailed vibrational analysis of this spectrum and similarly obtained RR spectra for TMPD-$d_4$, p-phenylenediamine$^{+\cdot}$ ($PPD^{+\cdot}$) and related compounds is in progress. For

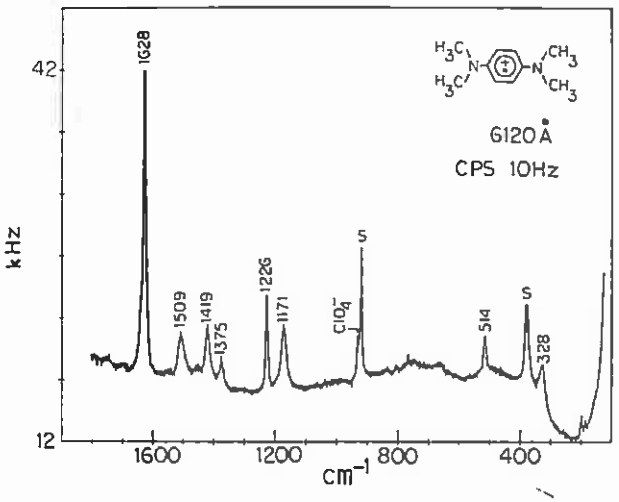


FIG. 9. — Resonance Raman scattering spectrum of electrogenerated $TMPD^{+\cdot}$ [TMPD] = 3.0 mM ; laser power = 35 mW ; bandpass = ca. 2 $cm^{-1}$ $TMPD^{+\cdot}$ was electrogenerated by cyclic potential step electrolysis at 10 Hz (see waveform in figure 7A) in 0.10 M TBAP/$CH_3CN$. The spectral scan rate was 0.333 3 Å $s.^{-1}$ using a 1.00 s. counting gate interval. Superradiant dye laser fluorescence was removed with a quartz prism Littrow mounted) pre-monochromator.

purposes of the present discussion it will be sufficient to simply identify the intense 1 628 $cm^{-1}$ feature as the totally symmetric benzene ring C = C stretching mode.

The time resolved feature of this experiment can be seen by setting the double monochromator at the maximum of the 1 628 $cm^{-1}$ scattering peak, applying the cyclic potential step waveform of figure 7 B with $\tau = 0.050$ s. and $\tau'/\tau = 19$, and collecting the digital resonance Raman intensity (RRI) *vs.* time transients in a 256 channel multichannel analyzer shown in figure 3. A typical RRI *vs.* time transient acquired in this manner is shown in figure 10. This signal required

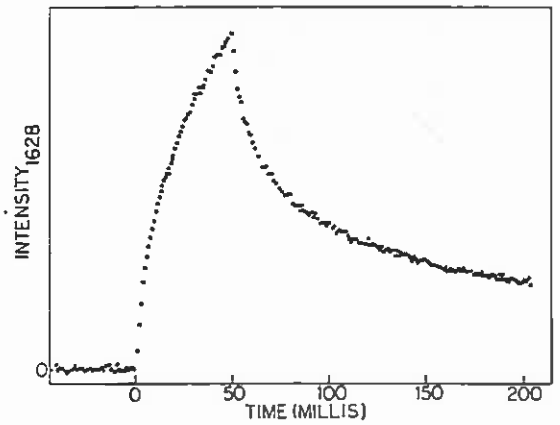


FIG. 10. — Signal averaged double potential step RRI *vs.* time profile for the 1 628 $cm^{-1}$ $TMPD^{+\cdot}$ band during the one-electron oxidation of TMPD. 1 000 averages ; 3.0 mM TMPD in 0.1 M TBAP/$CH_3CN$ ; R6G dye laser power at the front surface of the RRSE cell window = 35 mW at 6 120 Å ; spectrometer bandpass = 2.0 $cm^{-1}$ ; potential step limits = + 0.31 volts *vs.* SCE and — 0.09 volts *vs.* SCE ; $\tau = 0.050$ s. ; $\tau'/\tau = 19$ ; background has been subtracted out ; 256 data points.

16.67 min. to reach the S/N ratio shown. Quantitative analysis of the time dependence of the forward and reverse portions of this transient show excellent agreement with the expected linear RRI *vs.* $t^{1/2}$ (forward step) and linear RRI *vs.* $t^{1/2} - (t - \tau)^{1/2}$ (reverse step) behaviour [37]. Thus we have demonstrated that RRSE in this *off-the-electrode* scattering configuration can be used to obtain high resolution vibrational spectra of electrogenerated species in an electrode diffusion layer as well as quantitatively valid diffusion controlled transient responses to a signal averaged, double potential step waveform. As a result we can now assert that RRSE combines the highest resolution molecular spectroscopy with the fastest time response of any spectroelectrochemical technique presently known. The following applications of this method are now actively being pursued in our laboratory : 1) extension of the time scale of this technique down into the microsecond range by combining time-correlated single photon counting detection with high repetition rate 10-100 μs wide pulse electrolysis, 2) acquiring the RR spectra of small theoretically interesting radical ions which have short lifetimes ($< 10^{-2}$ s.) in their electrogeneration environment, and 3) using the quantitative RRI transients to monitor the kinetics of follow-up chemical reactions.

5. **Raman spectroscopy of an electrode/solution interface.** — The use of NR spectroscopy for probing the molecular structure of the electrode/solution interface has been quite effectively demonstrated by Fleischmann, Hendra, and McQuillan [13, 15, 16]. The most extensively studied system is that of neutral pyridine adsorbed on a silver electrode in aqueous solution containing 0.1 M KCl. Our interest in this topic in general and the results of Fleischmann, *et al.* in particular arose from our desire to apply the highly sensitivity RRS rather than NRS, which we initially expected was too insensitive, to the problem of *in situ* monitoring of the molecular structure of polarized interfaces. In order to gain familiarity with surface Raman spectroscopy and to provide some verification of Fleischmann's surprising results, we decided to repeat some of their experiments under our laboratory conditions [34, 39]. We were particularly interested in the intensity of the reported surface Raman signals since they appeared to be considerably greater than would have been predicted *a priori* on the basis of the known Raman scattering cross section of pyridine. Our measurements show that these surface signals can be considerably *more intense* than first reported. In fact by studying the experimental variables that influence the intensity of these signals such as : 1) method of electrode surface preparation ; 2) bulk solution concentration of pyridine ; 3) nature and concentration of the supporting electrolyte anion ; and 4) electrode potential, we were able to optimize the conditions for observing surface Raman signals. Under these optimized conditions, we find that the surface pyridine scattering intensity is on the order of $10^5$ *to* $10^6$ *times greater* than the corresponding scattering intensity from pyridine in solution. In addition we have studied the time response of the surface Raman signal to a double potential step waveform of the type shown in figure 7 B and have found that the surface scattering intensity is so large that we have the capability of monitoring the *in situ* time dependence of surface processes by Raman spectroscopy. Furthermore we have found that a wide variety of organic amines and nitrogen heterocyclic compounds produce high S/N ratio surface Raman spectra on silver electrodes and that it is possible to increase the sensitivity of the surface Raman technique still further by using adsorbates with a chromophore that can be resonantly excited by the laser source.

The surface Raman experiments to be described here were carried out in essentially an identical manner to that described by Fleischmann, *et al.* All experiments utilized the cell of figure 2 B with masked bulk silver wire electrodes. For most of the experiments, the 5 145 Å line of the $Ar^+$ laser was used as the excitation source although we have made some preliminary studies of the laser excitation frequency dependence of the surface Raman scattering process. In the case of 5 145 Å excitation (as well as all the other Ar laser lines and CW dye laser frequencies) pyridine is a NR scatterer since its absorption spectrum shows $\varepsilon = 0$ for all $\lambda \geqslant$ ca. 3 000 Å.

5.1 Optimization of the surface Raman signal for the pyridine/Ag system. — The strongest surface Raman signals from adsorbed pyridine on Ag were obtained with : 1) Ag surface preparation by mechanical polishing with 600 mesh $Al_2O_3$ followed by a single double potential step anodization of 2.0 s. duration from an initial potential of − 300 mV *vs.* SCE to + 200 mV *vs.* SCE in which 25 millicoulombs $cm^{-2}$ were passed in the forward step and 99.8 per cent of that charge was recovered in the reverse step ; 2) bulk pyridine concentration of 50 mM ; 3) $Cl^-$ supporting electrolyte concentration in a 2 : 1 ratio to the bulk pyridine concentration (i. e., 0.10 M) ; and 4) an applied electrode potential of between − 0.6 and − 0.8 V *vs.* SCE. Figure 11 shows full spectral scans from 100 $cm^{-1}$ to 3 400 $cm^{-1}$ for the $Ag/H_2O/Pyridine/Cl^-$ system under these optimized conditions in which we compare the surface background signal (upper panel), the bulk solution background signal (center panel) and the adsorbed pyridine surface signal at − 0.2 V *vs.* SCE (lower panel). Figure 12 shows that spectral variations are observed when the Ag electrode is potentiostated at increasingly negative applied potentials as would be required for a true surface signal and figure 13 gives a more quantitative picture of the relative intensity changes in the observed Raman bands as the applied potential is linearly swept from 0.0 volt to − 1.0 volt *vs.* SCE. In addition we find that the Raman intensity changes

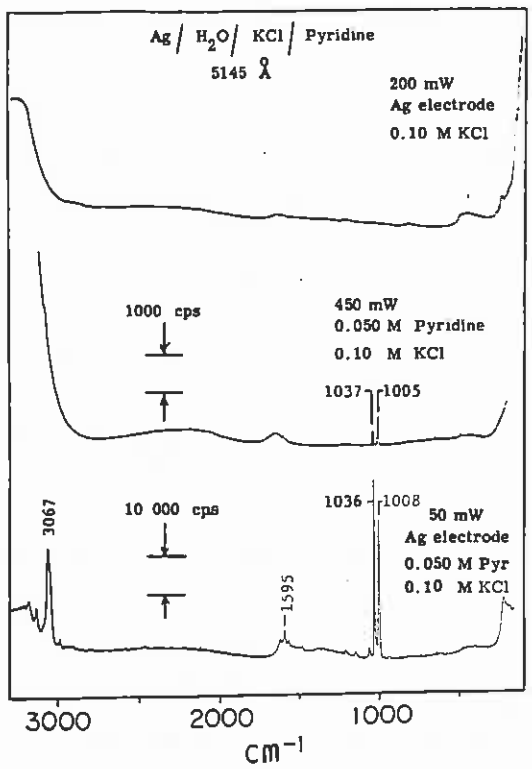


FIG. 11. — Top : Raman spectrum of a silver electrode immersed in 0.1 M KCl. Center : Raman spectrum of 50 mM aqueous pyridine and 0.1 M KCl. Bottom : Raman spectrum of pyridine adsorbed on a silver electrode from a bulk solution of 50 mM pyridine and 0.1 M KCl. Electrode potential = — 0.2 V *vs.* SCE. The electrode was prepared by a single anodizing pulse condition. All spectra were scanned at 0.333 3 Å/s. with a 2 $cm^{-1}$ bandpass and a 1.0 s. counting interval. Laser powers used were : *a*) 200 mw ; *b*) 450 mw ; and *c*) 50 mw. An interference filter was used to eliminate plasma line contributions to the spectra.

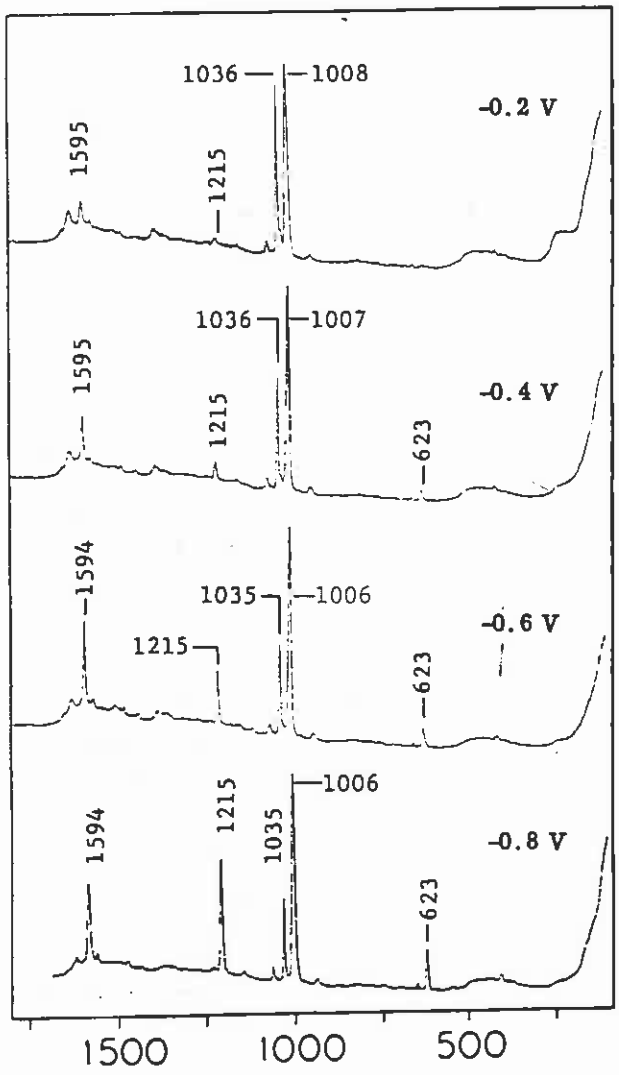


FIG. 12. — Raman spectra of pyridine adsorbed on a silver electrode from a solution of 50 mM pyridine and 0.1 M KCl. Electrode potentials are : — 0.2 V ; — 0.4 V ; — 0.6 V ; and — 0.8 V *vs.* SCE. The electrode surface was prepared according to our standard single pulse anodization procedure. The laser power was 80 mw at 5 145 Å. The spectra were recorded with a 2 $cm^{-1}$ bandpass with a 0.333 3 Å/s. scan speed and a 1.0 s. counting interval.

which are observed as the applied potential is made more negative occur as fast as the applied voltage waveform. This is demonstrated at least on the millisecond time scale by the potential step response of the surface Raman signal shown in figure 14. Comparison of the shape of the surface step response with that of a diffusion controlled bulk solution step response such as that shown in figure 10 indicates that the species responsible for these intensity changes is on the surface and not being diffusively transported in bulk solution. The most important observation to be reported here is that the intensity of the surface Raman spectrum is many times greater than that of the bulk solution signal. A simple calculation of the relative scattering efficiency of pyridine molecules on the surface compared to those in bulk solution illustrates this intensity difference. If one assumes a monolayer coverage of the electrode, 38 $Å^2$ $molecule^{-1}$ [40], and a real surface area of $7.5 \times 10^{-3}$ $cm^2$ intercepted by a laser beam focused to an image of 50 $\mu \times 3$ mm (i. e., a surface roughness factor = 5), $2 \times 10^{12}$ pyridines are participating in the surface scattering. In the solution case with the same laser focusing conditions and the beam passing through a 1 mm cell containing 50 mM pyridine, $4.5 \times 10^{15}$ pyridines participate in scattering. Correcting for the fact that 50 mW of laser power produces a 36 000 Hz signal in the surface case and 450 mW of laser power is required to produce a solution signal of 700 Hz, one concludes that a monolayer surface signal is $10^6$ times more intense than the solution signal and if 10 monolayers were in fact on the surface under these conditions the surface signal would still be $10^5$ times more intense than the solution signal.

5.2 SUMMARY OF OTHER OBSERVATIONS. — There are slight differences in the spectroscopic characteristics of the surface pyridine species as compared to bulk pyridine species. There are, for example, small but measurable shifts in certain of the prominent band

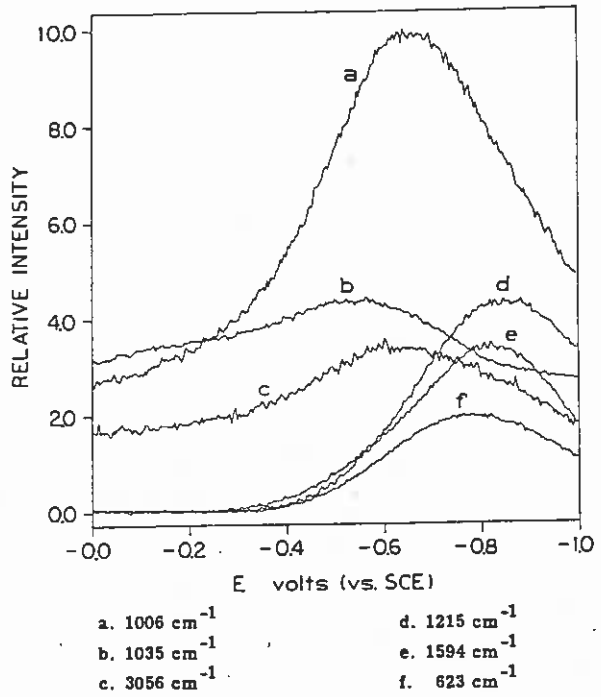


FIG. 13. — Raman intensity dependence due to adsorbed pyridine as a function of electrode potential. The electrode surface was anodized under our standard single pulse conditions. A relatively large spectrometer bandpass (20 $cm^{-1}$) was used to minimize the error in intensity measurement due to the effect of band frequency changes with electrode potential. Laser excitation wavelength = 5 145 Å. The electrode potential was scanned at a rate of 1.024 V/s. beginning at 0.0 V *vs.* SCE. Each curve was signal averaged over ten potential scans.

positions (viz., 1 037 $cm^{-1}$ in solution *vs.* 1035 $cm^{-1}$ on the surface or 3 076 $cm^{-1}$ in solution and 3 056 $cm^{-1}$ on the surface). The depolarization ratios of the surface signals are vastly different from the corresponding solution bands (viz., for the 1 005 $cm^{-1}$ band in solution $\rho = 0.03$ whereas for the 1 008 $cm^{-1}$ surface band $\rho = 0.64$). In addition we cannot observe any significant departure from an $\omega_S^4$ excitation frequency dependence as might be expected if a resonance Raman process of the type described in section 2 was operative here. We tentatively conclude that we are observing a NR process that is enhanced by a different mechanism for these surface species.

Other observations include several chemical variations. The intensity of the surface Raman signal varies with the nature of the supporting electrolyte anion in a manner reminiscent of the order of specific anion adsorption

$$(\text{viz., } I^- \gg Br^- > Cl^- > NCS^- > HPO_4^- > SO_4^{=} \gg ClO_4^-)\,.$$

No strong surface Raman signals are observed at nonaqueous solvent/electrode interfaces. We have observed surface Raman spectra only at Ag and Cu electrodes as reported by Fleischmann [16]. We have not seen spectra for aqueous pyridine/Pt, Au, Pb, or

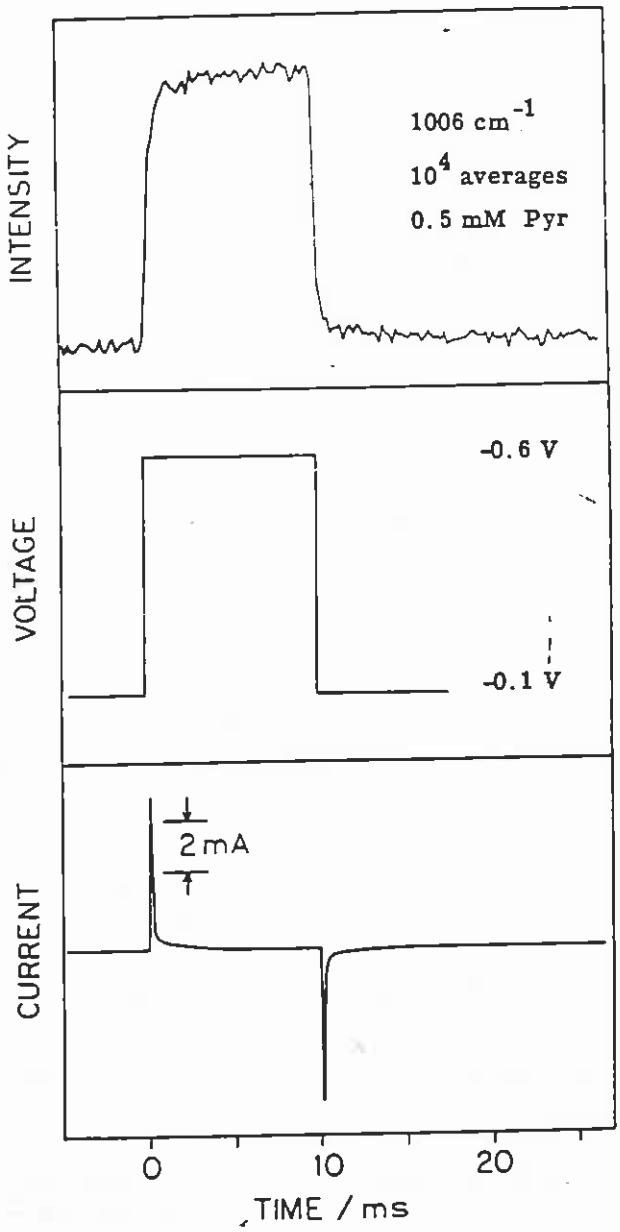


FIG. 14. — Top : Raman time response of the intensity due to the 1 006/1 008 $cm^{-1}$ band of adsorbed pyridine on a silver electrode where the initial potential is — 0.1 V (SCE) and the step is to — 0.6 V for a duration of 10 ms. with a 20 % duty cycle. The electrode was prepared under our standard single pulse anodization conditions in the presence of a 0.5 mM bulk concentration of pyridine and a 0.1 M KCl supporting electrolyte concentration. Center : Double potential step voltage waveform input to the potentiostat. Bottom : Electrochemical cell current for the above potential step.

Cd interfaces. We have varied the nature of the adsorbate and found that other pyridine derivatives give rise to strong surface spectra (viz., 4-cyanopyridine and 2, 4, 6-trimethyl-pyridine). In contrast pyrazine gives only a very weak spectrum. Organic amines with only 1 N such as aniline and N, N′-dimethylaniline give strong spectra ; whereas, amines with two symmetrically placed N's such as p-phenylenediamine gives no spectrum. $\pi$-Electrons are not a prerequisite

for observing surface spectra since the saturated analog of pyridine, piperidine, and the aliphatic amine, benzylamine, give strong surface spectra. We conclude that the strongest interaction between pyridine (or piperidine) and the Ag surface is through the N lone pair and thus the configuration giving rise to the surface Raman spectra is probably a *perpendicularly* bound pyridine (Ag-N interaction) rather than a *flat* pyridine (Ag-$\pi$ interaction). When two N's are available for surface binding such that the lowest energy form for the adsorbate is the *flat* configuration, only a weak surface signal or no surface signal is observed. The final chemical variation that will be presented here is a preliminary experiment in which a molecule with a chromophore that can undergo the conventional RR process is adsorbed on the Ag surface. The test molecule was the dye crystal violet and as one can see in figure 15 an extremely intense (i. e., high S/N) spectrum was observed even though only 1 mW of 5 145 Å laser power was incident on the electrode surface. This suggests that it may be possible to combine the surface enhancement process, whatever its detailed nature, with a conventional RR enhancement process to achieve a net increase in Raman scattering efficiency over the conventional bulk solution NR process of the order of $10^8$ to $10^9$.

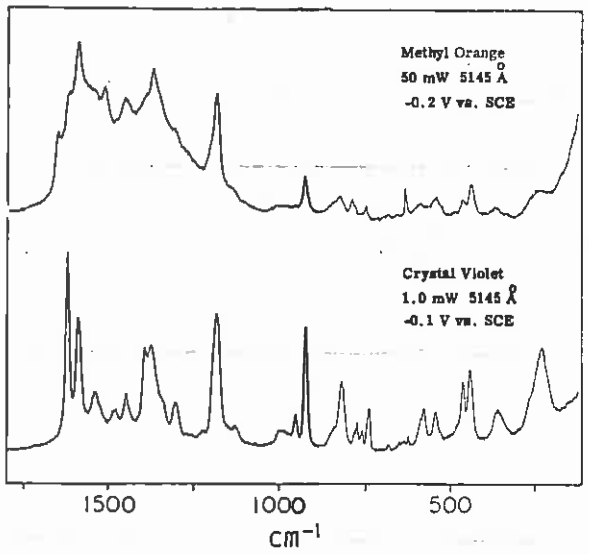


FIG. 15. — Top : Methyl orange adsorbed on a silver electrode. Electrode potential = — 0.2 V *vs.* SCE, and the laser power = 50 mw. The bulk solution contains only a trace amount of methyl orange. Bottom : Crystal violet under the same conditions as above except the electrode potential is — 0.1 V *vs.* SCE and the laser power = 1.0 mw. Laser excitation wavelength for both spectra = 5 145 Å.

5.3 CONCLUSIONS CONCERNING THE ORIGIN OF THE HIGH INTENSITY SURFACE RAMAN SIGNALS. — The physical origin of these high intensity surface Raman signals is not known with certainty at this time. Whatever the mechanism of the surface enhancement is, it must be able to account for the following experimental facts : 1) the magnitude of the effect is very large ca. $10^5$ to $10^6$ ; 2) the enhancement mechanism exhibits an apparent orientational preference for molecules which adsorb *end-on* or *perpendicular* to the electrode surface as opposed to those that adsorb in a *flat* configuration ; 3) the depolarization ratios of the surface signals are vastly different from those of the corresponding Raman lines in solution and in all cases measured so far the depolarization ratio of the surface signal is ca. 0.6-0.7 as compared to 0.01-0.03 for the solution signal ; 4) the number of Raman lines observed and their relative intensities are strong functions of the applied potential ; 5) there is no strong departure from the $\omega_S^4$ excitation frequency dependence over the range 4 579 Å to 6 500 Å that would be associated with a NR scattering process ; and 6) in cases such as pyridine adsorption where the adsorbate in bulk solution dœs not absorb the excitation light, the surface Raman signals are stable as a function of time (for the duration of at least one monochromator scan i. e., at least 1 hour) even at quite high laser power (i. e., up to a few hundred milliwatts incident on the surface). In addition to unraveling the physics of the surface Raman enhancement process, a chemical model of the Raman active species at the interface must be proposed to account for the observed sensitivity to such chemical variables as the electrode material, supporting electrolyte anion, and its concentration.

In figure 16 we schematically illustrate a tentative model for the structure of the Raman active species at the electrode/solution interface. We believe that *perpendicularly* bound pyridine stabilized by 2 specifically adsorbed $Cl^-$ ions per pyridine is the Raman active surface species. This model accounts in a simple way

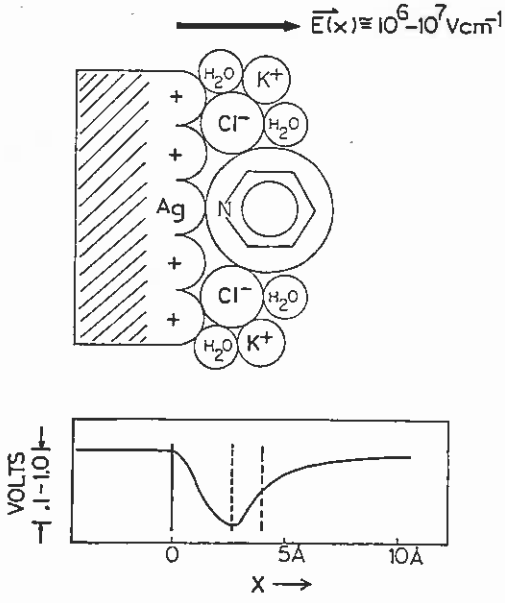


FIG. 16. — Schematic diagram of a tentative model for structure of the electrode/solution interface including the distance dependence of the interfacial electric field.

for the sensitivity of the observed intensity to the nature and concentration of the supporting electrolyte anion. The fact that silver electrodes show the largest surface Raman intensity can be partially accounted for by the fact that : 1) it has the most negative point of zero charge (pzc) and therefore the largest amount of adsorbed $Cl^-$ at a given potential of the metals tested and 2) if one assumes that $Cl^-$ induced adsorption of pyridine occurs in such a way as to preferentially stabilize the perpendicular orientation of the adsorbate. On this basis it is difficult however to account for the absence of surface Raman signals on Au since $Cl^-$ is also quite strongly adsorbed on Au, at least as detected by ellipsometriy [41], but perhaps not strongly enough adsorbed (i. e., a delicate balance of factors may be involved).

With regard to the physics of the surface enhancement process at least two hypotheses can be put forward : 1) the surface species are exhibiting a resonance Raman enhancement of the type discussed in section II in which there is a substantial broadening of the excited state electronic energy levels of adsorbed pyridine at these rough silver surfaces so that resonance Raman scattering is induced through interaction with surface plasmons [42], and 2) the normal Raman scattering cross section of the adsorbed pyridine molecules is being enhanced by the extremely large interfacial electric field gradient, $10^6$-$10^7$ V $cm^{-1}$ present in the double layer region [43]. Although there is presently inadequate data available to unambiguously distinguish between these hypotheses, I tend to favor more the electric field enhancement hypothesis or at least some combination of electric field and surface plasmon induced RR scattering since electric field enhancement could account in a simple way for : 1) the orientational sensitivity of the effect, 2) the sensitivity to applied potential, and 3) the fact that no strong dependence of excitation wavelength is observed. In addition one can cite a recent paper by Aussenegg, *et al.* [44] in which the intensity of normal Raman scattering from simple liquids such as benzene and $CS_2$ was measured as a function of applied electric field strength over the range 0-7 $\times$ $10^5$ V $cm^{-1}$. They found that at the highest field strengths obtainable in their apparatus, which are about a factor of 15 below the field strengths that can be encountered by pyridine in the electrical double layer, the intensity of the 648 $cm^{-1}$ totally symmetric stretch of $CS_2$ was a factor of about 6 more intense in the presence of the field than in its absence. In addition they found that the depolarization ratio for this mode was approaching 0.75 at high fields as compared to 0.22 in the absence of the field. In all cases they found a larger value of the depolarization ratio in the presence of the field than in its absence. Although this report by Aussenegg does not prove an electric field enhancement mechanism is operative in the case of pyridine adsorbed on silver electrodes, it does indicate that large electric fields could account for our observed behaviour. Although the surface plasmon induced RR scattering hypothesis would not account for the orientational sensitivity of our observations, I would expect that one would observe a significant departure from $\omega_S^4$ scattering behaviour and that one would not observe stable signal intensities at high incident laser power since if an absorption process is occurring and the energy absorbed is dissipated as heat, one might expect significant surface damage such as we do, in fact, observe when we intentially adsorb an RR scattering species such as crystal violet on the silver electrode. In any event I believe that we have unambiguously demonstrated that the surface Raman signals are many orders of magnitude more intense than their solution counterparts and that more detailed experiments are required to establish the nature of this very interesting enhancement mechanism. It is hoped that once the nature of this mechanism is understood it can be controlled and utilized in such a way that surface Raman spectroscopy at solid/liquid interfaces becomes a general tool for the study of the fascinating and important chemical phenomena that take place in such environments.

**Acknowledgements.** — The author is indebted to his coworkers Dr David L. Jeanmaire and Dr Mary R. Suchanski and to the National Science Foundation whose generous support through Grants CHE74-12573 A03 and CHE75-15480 has made this research possible. In addition I would like to acknowledge Professor Charles Harris (Berkeley) and Dr Michael R. Philpott (IBM San Jose) for helpful discussions concerning the nature of the surface Raman enhancement process.

## References

[1] KUWANA, T., *Ber. Bunsenges. Phys. Chem.* 77 (1973) 858.
[2] LASER, D. and ARIEL, M., *J. Electroanal. Chem.* 41 (1973) 381.
[3] ALLENDOERFER, R. D., MARTINCHEK, G. A. and BRUCKENSTEIN, S., *Anal. Chem.* 47 (1975) 890.
[4] RICHARDS, J. A. and EVANS, D. H., *Anal. Chem.* 47 (1975) 964.
[5] PETEK, M. and BRUCKENSTEIN, S., *J. Electroanal. Chem.* 47 (1973) 329.
[6] MCINTYRE, J. D. E., Advances in Electrochemistry and Electrochemical Engineering, Vol. 9 (Wiley and Sons, New York) 1973.
[7] HANSEN, W. N., Advances in Electrochemistry and Electrochemical Engineering, Vol. 9 (Wiley and Sons, New York) 1973.
[8] MULLER, R. H., Advances in Electrochemistry and Electrochemical Engineering, Vol. 9 (Wiley and Sons, New York) 1973.
[9] KIM, K. S., WINOGRAD, N. and DAVIS, R. E., *J. Am. Chem. Soc.* 93 (1971) 6296.
[10] JOHNSON, W. G. and HELDT, L. A., *J. Electrochem. Soc.* 121 (1974) 34.
[11] SHIBATA, S., *Electrochim. Acta* 17 (1972) 395.

[12] JEANMAIRE, D. L., SUCHANSKI, M. R. and VAN DUYNE, R. P., *J. Am. Chem. Soc.* 97 (1975) 1699.
[13] FLEISCHMANN, M., HENDRA, P. J. and MCQUILLAN, A. J., *Chem. Phys. Lett.* 26 (1974) 163.
[14] CLARKE, J. S., KUHN, A. T. and ORVILLE-THOMAS, W. J., *J. Electroanal. Chem.* 54 (1974) 253.
[15] MCQUILLAN, A. J., HENDRA, P. J. and FLEISCHMANN, M., *J. Electroanal. Chem.* 65 (1975) 933.
[16] FLEISCHMANN, M., HENDRA, P. M., MCQUILLAN, A. J. and PAUL, R. L., *J. Electroanal. Chem.* 66 (1975) 248.
[17] TANG, J. and ALBRECHT, A. C., Raman Spectroscopy — Theory and Practice, Vol. 2 (Plenum, New York) 1970.
[18] MINGARDI, M. and SIEBRAND, W., *J. Chem. Phys.* 62 (1975) 1074.
[19] VAN DUYNE, R. P. and JEANMAIRE, D. L., *J. Am. Chem. Soc.* 98 (1976) 4034.
[20] ALBRECHT, A. C. and HUTLEY, M. C., *J. Chem. Phys.* 55 (1971) 4438.
[21] KONINGSTEIN, J. A., Introduction to the Theory of the Raman Effect, D. Reidel (Dordrecht, Holland) 1972.
[22] SPIRO, T. G., *Acc. Chem. Res.* 7 (1974) 339.
[23] MINGARDI, M., SIEBRAND, W., VAN LABEKE, D. and JACON, M., *Chem. Phys. Lett.* 31 (1975) 208.
[24] SUCHANSKI, M. R., Ph. D. Thesis, Northwestern University, Evanston, Illinois (1977).
[25] DONZEL, A. and WEISBUCH, C., *Opt. Commun*, 17 (1976) 153.
[26] WALLACE, R. W., *Appl. Phys. Lett.* 17 (1970) 497.
[27] VAN DUYNE, R. P. and FISCHER, S. F., *Chem. Phys.*, 5 (1974) 183.
[28] EFRIMA, S. and BIXON, M., *Chem. Phys. Lett.* 25 (1974) 34.
[29] EFRIMA, S. and BIXON, M., *J. Chem. Phys.* 64 (1976) 3639.
[30] ULSTRUP, J. and JORTNER, J., *J. Chem. Phys.* 63 (1976) 4358.
[31] EFRIMA, S. and BIXON, M., *Chem. Phys.* 13 (1976) 447.
[32] ROUSSEAU, D. L. and WILLIAMS, P. F., *J. Chem. Phys.* 64 (1976) 3519.
[33] JEANMAIRE, D. L. and VAN DUYNE, R. P., *J. Am. Chem. Soc.* 98 (1976) 4029.
[34] JEANMAIRE, D. L., Ph. D. Thesis, Northwestern University, Evanston, Illinois (1977).
[35] BERLINSKY, A. J., HOYANO, Y. and WEILER, L., *Chem. Phys. Lett.* 45 (1977) 419.
[36] ZAHRADNIK, R., CARSKY, P., HUNIG, S., KIESSLICH, G. and SCHEUTZOW, D., *Int. J. Sulfur Chem.* Part C. 6 (1971) 109.
[37] JEANMAIRE, D. L. and VAN DUYNE, R. P., *J. Electroanal. Chem.* 66 (1975) 235.
[38] ALBRECHT, A. C., *Acc. Chem. Res.* 3 (1970) 238.
[39] JEANMAIRE, D. L. and VAN DUYNE, R. P., *J. Electroanal. Chem.* (1977) in press.
[40] BARRADAS, R. G. and CONWAY, B. E., *J. Electroanal. Chem.* 6 (1963) 314.
[41] PAIK, W., GENSHAW, M. A. and BOCKRIS, J. O. M., *J. Phys. Chem.* 74 (1970) 4266.
[42] PHILPOTT, M. R., *J. Chem. Phys.* 62 (1975) 1812.
[43] MOHILNER, D. M., Electroanalytical Chemistry, Vol. 1 (Marcel Dekker, New York) 1966.
[44] AUSSENEGG, F., LIPPITSCH, M., MOLLER, R. and WAGNER, J., *Phys. Lett.* 50A (1974) 233.

## DISCUSSION

E. YEAGER (a comment). — Dr. Hagen of the University of Trondheim worked in our laboratory last year and confirmed the strong Raman signal of adsorbed pyridine on Ag electrodes. His finding parallel in good part those presented by Dr. Van Duyne in his lecture, and by the university of Southampton group. Dr. Hagen also examined p-nitrosodimethylaniline (PNDA) which exhibits a strong resonant enhancement in bulk solution at the 488.0 nm argon laser line and to a lesser extent (10 foldless) at the 5 145 nm line. A strong Raman signal was found for this species adsorbed on Ag electrodes in chloride and also in sulfate solution with the over signal of almost equal strength for both of the argon laser lines. In contrast a strong Raman signal was found for the species adsorbed on Pt in chloride solution only at 488.0 nm. The relative peak heights and shapes in the Raman lines in the range 1 000-1 200 $cm^{-1}$ for the adsorbed PNDA diffused from those for both solution and were potential dependent.

S. GOTTESFELD (comment). — Is response to the remark by Dr. Aguis. I would like to point out that in recent measurements on mechanically (in-situ) abraded Ti electrodes we found that for Ni oxide films thinner than 100 Å, combination of ellipsometric and reflectometric results gave, after a least square analysis, optical properties quite close to those of bulk intrinsic rutile ($\hat{n} \approx 2.40 - 0i$). It thus seems that mechanically polished electrode does not always yield apparent high values of $k$, which are the most natural result of a roughened metal surface.